Variability of the eastward currents in the equatorial Atlantic during 1993-2011

Marlos Goes [1,2*], Gustavo Goni[1], and Verena Hormann[1,2], Renellys Peres[1,2]

To be submitted to Journal of Geophysical Research

1 Atlantic Oceanic and Meteorological Laboratory, National Oceanic and Atmospheric Administration, Miami, FL 33149, USA.

2 Cooperative Institute for Marine and Atmospheric Studies, University of Miami, Miami, FL 33149, USA.

Abstract

We develop, validate and apply a synthetic method to monitor the equatorial currents in the Atlantic. This method uses high-density expendable bathythermograph (XBT) data from the AX08 transect and satellite altimetry to estimate properties of the currents and their variability in seasonal and interannual timescales. The method is well suited for surface currents, such as the North Equatorial Countercurrent (NECC), and has some skill in resolving the variability of North Equatorial Undercurrent (NEUC). The synthetic method fails to describe the variability of the South Equatorial Undercurrent (SEUC), which located in a region of small sea surface height variability. Our results confirm that the NECC shows a strong annual cycle of transport, with high values from July-December, and shows a possible strengthening (1-2 Sv on average) in the 2000 decade in comparison with the 1990s. On interannual time-scales, there is a positive correlation between the NECC transport and an anomalous sea surface temperature north-south gradient and the strengthening of the southwesterly winds. The NEUC shows a stronger transport values up to 10 Sv from January-July, and the interannual variability of the NEUC transport agrees with previous mechanisms such that it is correlated with the sea surface temperature on the Gulf of Guinea and southeastern equatorial bands, and reduction of equatorial winds. The EUC shows strong annual and semi-annual component of its variability in the region. This study shows that for a long-term monitoring system of the region, both altimetry and XBT data are necessary a near-real-time inference of the dynamical and thermodynamical properties of the current system in the tropical Atlantic region.

1. Introduction

The tropical Atlantic current system is of great importance for both inter-hemispheric and west-to-east exchange of heat and nutrients, which also impacts the climate and weather in the surrounding continental areas [e.g., McCready et al., 2002; Goldenberg et al., 2001; Sutton and Hodson, 2005].

In the upper tropical Atlantic, the main conduit for the inter-hemispheric water exchange is the North Brazil Undercurrent/Current (NBUC/NBC), which is a western boundary current system. On its northward path, part of the NBC retroflects eastward and feeds into a system of zonal countercurrents [Schott et al., 1995; Bourles et al., 1999a]. Specifically, into the Equatorial Undercurrent (EUC) along the equator, and three off-equatorial currents, the North Equatorial Countercurrent (NECC), the North Equatorial Undercurrent (NEUC), and to a lesser extent the South Equatorial Undercurrent (SEUC).

The EUC has been largely studied for being unique in terms of its dynamics [e.g., Pedlosky, 1987] and for being strongly related to the equatorial upwelling, and the Atlantic zonal mode [e.g., Goes and Wainer, 2003; Hormann and Brandt, 2007]. The seasonal cycle of the EUC has been analyzed in a model simulation [Arhan et al., 2006], in which two transport maxima of the EUC were found in the central part of the basin, one during boreal fall and another during summer. They suggested that two different dynamical regimes drive the EUC seasonal cycle: in summer and fall, the simulated EUC is mostly driven by equatorial zonal forcing, and supplied from the ocean interior; in winter and spring, it is driven by remote forcing through the rotational wind component, and supplied from the western boundary currents.

In regard to the off-equatorial currents, the NECC, for having a strong surface signature, has also been widely studied. This current is mainly located between 3-10°N [Garzoli and Katz, 1983; Richardson and Walsh, 1986], with its seasonal variability linked to the migration of the Intertropical Convergence Zone (ITCZ) [e.g., Fonseca et al., 2004]. The NECC is forced mostly by wind stress within the equatorial band, either by local wind stress curl (WSC) or wave mechanisms. In addition, the NECC plays an important role in the global meridional overturning circulation [Frantantoni et al., 2000], since part of its flow is carried through Ekman transport northward, contributing to the meridional heat transport.

The off-equatorial undercurrents (OEUCs), though, are still not widely understood. They contribute to the shallow subtropical overturning cells that link the subtropical subduction regions to the equatorial and coastal upwelling regions. The OEUCs provide cold subthermocline water for the off-equatorial eastern upwelling regimes along the African coast, more specifically for the Guinea and Angola Domes [Schott et al. 2004; Doi et al., 2007]. Recent advances in understanding the Atlantic OEUCs are presented, for example, in Huettl-Kabus and Boening [2008] and Fischer et al. [2008]. It is important to study the variability of the OEUC, for instance, because of their contribution to the zonal transport of nutrients such as O_2 through long distances [Brandt et al. 2008]. The OEUCs are located below the thermocline coincident with the equatorial thermostad, at about 3–6° of latitude. The SEUC is mostly fed by internal recirculations [Schott et al. 1995, 1998], and according to Reverdin et al. [1991], its seasonal cycle at 30°W is characterized by a maximum transport in the boreal fall and a minimum in boreal spring. Close to its origin, the SEUC flow consists of large standing meanders [Fischer et al., 2008]. The NEUC is weaker than the SEUC, and also more variable. For instance, Schott et al. [2003] used an average of 13 shipboard sections at 35°W, and stated as uncertain the existence of the NEUC. Indeed, the SEUC and NEUC show a large intra-seasonal variability linked to tropical instability wave activity [Jochum et al., 2003], and instabilities are more prominent in the northern hemisphere [Athie and Marin, 2008; Foltz et al., 2004b]. In the central basin, the separation between the NECC and NEUC is not very clear, but the NEUC may present higher transport values in boreal spring. On the western side of the basin, some studies [e.g., Bourles et al., 1999; Goes et al., 2005] report only one eastward current core within the thermostad (between 100–250 m) that is comprised of waters from both the northern and southern hemispheres. Therefore, the EUC and NEUC may originate from this single core, and split into two cores with different water mass properties further east.

Several mechanisms may be responsible for the variability of the OEUCs. The tropical instability waves (TIWs) may drive intraseasonal variability of the OEUCs and the variability of their meridional displacement [Rowe at al., 2002]. Diffusive processes are important to the balance of the momentum of the OEUCs [McPhaden, 1984; Johnson and Moore, 1997], and the TIWs play an important role on the maintenance of the OEUCs as they act as a necessary source of heat flux and momentum, therefore explaining the rise of the OEUCs across the isopycnals [Jochum and Malanotte-Rizzoli, 2004]. Remote forcings are also vital for the onset and maintenance of the OEUCs. From these forcings we can include the upwelling in the eastern side of the basin [McCreary et al., 2002; Doi et al., 2007], the global thermohaline circulation [McCreary et al., 2002; Furue et al., 2007], and the subtropical cells [Marin et al., 2003; Hua et al., 2003].

Due to the high variability in the region, it is imperative to have an observational system that can resolve mesoscale features as well as the temporal structure of the currents. This can be realized through current meters and cruise data at a relatively high cost. One potential candidate for a sustainable observational system that resolves reasonably well the spatial and temporal scales, and presents a large spatial coverage is satellite altimetry. However, there are substantial upper-ocean currents with very weak sea surface signatures and spatial variability that cannot be resolved from surface topography fields alone [Goni and Baringer, 2002]. This deficiency can be overcome by establishing a relationship between certain current bands and their characteristic sea surface height signature. This can be performed by using altimetry in combination with other observational platforms such as high-resolution hydrographic data. Therefore, a reliable monitoring system for the region requires complementary platforms in order to produce details of the spatial and temporal variability [Goni and Baringer, 2002].

The high-density (HD) XBT project has been active for over 20 years, and aims at sustainably measuring physical properties of the upper ocean with mesoscale resolution. Its high spatial data resolution and repeated sampling of the region enable assessing upper-ocean properties such as temperature variability and heat storage, and permit the characterization of the variability of the major geostrophic currents.

The goal of this study is to quantify the variability of the eastward currents in the equatorial Atlantic during 1993-2011, and determine properties such as transport, velocity and location of these currents. More specifically, we focus on the seasonal and interannual signatures of the NECC, EUC, and OEUCs manifested in observations. To accomplish this goal, we consider a monitoring system that comprises data from the XBT transect AX08 between the years 2000-2011, and uses altimetry to synthetically quantify the variability of the eastward currents in the equatorial Atlantic for the 1993-2011 period. The validity of the synthetic method and future prospects are also assessed in this study.

Henceforth, this paper is structured as follows: first we describe in detail the data to be used and introduce the methodology (Section 2); in Section 3 we validate the synthetic method and apply it to study the seasonal and interannual cycles of the eastward equatorial currents, and analyze the surface response and forcings linked to the variability of these currents. Discussion, conclusions and recommendations for future work are provided in the final section of the paper.

2. Data and methods

This work uses mainly two observational platforms to infer the variability of the Atlantic eastward equatorial current system: the AX08 HD XBT transect and satellite altimetry data. Specifications of each of these datasets as well as additional data used are given below.

a) Hydrographic data

The temperature data used in this study are from 39 realizations of the AX08HD XBT transect, which spans between Cape Town and New York City since 2000, crossing the equator at about 23°W (Figure 1c). An average of four transects per year has been achieved since 2002, with about 200-300 XBTs deployed on each transect, and a spacing of about 25 km between consecutive deployments in the tropics.

Individual temperature profiles are interpolated linearly to a 2 m resolution in depth for the upper 800 m. The data are quality controlled by excluding the profiles whose horizontal gradients lie outside the three standard deviation range of all profiles. Next, the sections are horizontally interpolated to a 25 km resolution (along track) in latitude, using an optimal interpolation procedure with a Gaussian correlation function with a decorrelation length scale of 200 km and a low observational error of 0.01. This procedure produces evenly spaced and smoother data. Salinity is inferred from temperature profiles using the climatological T-S relationships from the World Ocean Database (WOD01, Conkright et al. [2002]).

Salinity profiles are extrapolated to the surface using a slab-layer approximation in the mixed layer. This is a standard approximation to overcome the non-unique characteristic of the T-S relationship in the tropical surface waters [Goes et al, 2005; Schott et al., 1998]. Goni and Baringer, [2002] has shown that differences between in-situ and climatological salinity are of the order of 0.3-0.4 psu, and the resulting uncertainty is among the largest contributors to the dynamic height error, with differences as large as 5 cm. This error is on the order of the sensitivity of our interpolation procedure, as well as on the order of the errors in the altimetric data [Cheney et al., 1994] used in our synthetic methodology described below.

We further explore the effect of the salinity on the steric height variability in the region by calculating the thermosteric and halosteric contributions to the total surface steric variability in three different latitudes, 4.5°N, 4.5°S and the equator (Figure 4) along the XBT transect. This calculation is performed using the methodology described in Foffonof and Froese [1955], and Tabata et al. [1986], in which departures from the mean sea level are estimated in terms of one component by keeping the other component fixed at its annual mean. The sum of the thermosteric and halosteric components is equal to the total steric variability of the XBT data. We illustrate their variability by showing the surface dynamic height (DH_0) referenced to 800 m.

In all three latitudes, the contribution due to halosteric variability to the variability of DH_0 is small, generally of the order of 1-2 cm. The variability of DH_0 closely follows the thermosteric variability in all latitudes. Salinity has a higher contribution to the total variability at the equator and at 4.5°S, where the total DH_0 variability is small. At those latitudes, the halosteric component count for 20-30% of the total variability. At 4.5°N, where there is high thermosteric variability with amplitude of ~30 cm, only ~10% of the DH_0 variability is due to the halosteric component.

The typical distribution of temperature and salinity along the AX08 section is exemplified by the months of January and July of 2010 (Figure 2). This region is characterized by a warm well-mixed layer in the top 100 m, followed by a sharp temperature gradient of the upper thermocline of approximately 0.1°C/m. North and south of the displayed domain are characterized by high salinity values around 100 m, within the upper thermocline waters. The high salinity waters are characteristic of the Subtropical Underwaters (SUW). SUWs are formed in the subtropics and advected equatorward by the North and South Equatorial Currents (NEC and SEC, respectively). Underneath the SUW are the central waters, characterized by the nearly straight line in the T-S space. These waters form the thermostad between 15°C and 12°C found in the equatorial region [Reverdin et al., 1991], which is more pronounced in the southern hemisphere between 5°S and the equator at around 200 m depth (Figure 2), and are coincident with the position of the OEUCs. Therefore, the central waters are the main source of waters for the OEUCs, particularly the SEUC. The NEUC is known to have also a strong contribution from the high salinity SUW. This is an important feature of the region, and confirms the higher contribution of the western boundary to the NEUC, and higher contribution from eastern waters to the SEUC. In fact, previous works [e.g., Schott at al. 1995, 1998] suggest that the source waters for the SEUC originate from a recirculation gyre.

b) Remote sensed data

Satellite altimetry provides global coverage of the sea surface height anomaly (SSA) relative to the 1993-1999 mean period. Here we use the AVISO delayed mode product (http://www.aviso.oceanobs.com), which consists of gridded SSA relative to the 1992-1998 period mean, obtained from a multi-satellite mission [Le Traon et al., 1998]. The delayed mode data are available continuously in a weekly temporal resolution since October 1992, on a 1/3° horizontal grid, with precision of 2 cm [Ducet et al, 2000; Cheney et al., 1994]. For the purpose of this study, we use data from October 1992-December 2010, subtracted the 2000-2011 period mean from the SSA field, and interpolate the data onto a Mercator grid with 0.25° x 0.25° resolution. Time and spatial liner interpolation is further applied when comparing to the XBT track locations.

We perform additional analysis using gridded sea surface temperature (SST) and pseudo-wind stress anomalies, averaged to monthly means and interpolated onto a 1°x1° mercator grid. The SST data used is the optimum interpolation (OISST-v2) analysis produced weekly on a one-degree grid [Reynolds et al., 2002]. The reanalysis uses in situ and satellite SST plus SST simulated by sea ice cover. Before the reanalysis is computed, the satellite data is adjusted for biases using the method of Reynolds [1988] and Reynolds and Marsico [1993], which improves the large scale accuracy of the OI.

The pseudo-wind stress data is taken from cross-calibrated, multi-platform (CCMP), multi-instrument ocean surface wind velocity data set, available since July 1, 1987. This data set combines data derived from SSM/I, AMSRE, TRMM TMI, Quikscat and other missions using a variational analysis method (VAM) to produce a consistent record of ocean surface vector winds at a 25 km resolution [Atlas et al. 1996].

Velocity calculation

In order to study the variability of the eastward equatorial currents, we restrict the observations to a region with similar dynamical characteristics. We define a criterion that selects the sections whose mean longitude lie within the 68 percentile around their median value between 10°S-10°N (Figure 1a). The median longitude of the transect, which is about 40° oblique with respect to a true meridional section, is approximately 23°W. Our selection reduces the number of transects from 39 to 32, but assures that we are dealing with comparable data.

Geostrophic currents are inferred from the hydrographic data using the thermal wind relationship (cf. Figure 3), which is the standard dynamical method to calculate velocities from this type of data. The cross-sectional velocity field is calculated from the horizontal gradients of dynamic height. We estimate absolute velocities by using the XBT dynamic heights relative to 800 m (DH_{XBT}), which the maximum depth reached by the XBTs, plus information about the absolute dynamic height at 800 m (DH_{IPRC}):

$$DH(z) = DH_{XBT}(z) + DH_{IPRC}(800), \tag{1}$$

where $DH_{IPRC}(800)$ is taken from the monthly of International Pacific Research Center (IPRC) climatology (http://apdrc.soest.hawaii.edu). This dataset is available on a 1°x1° horizontal grid at 27 depth levels derived from ARGO floats and altimetry observations, with mean sea level referred to MDT_CNES-CLS09 [Rio et al., 2011]. The inclusion of $DH_{IPRC}(800)$ reduces considerably the mean DH (~ 70 cm), but the DH gradients are not greatly affected (< 1 cm). In the equatorial region, geostrophy has an inflection point, and it is necessary to use the equatorial beta approximation, which relies on the calculation of higher order derivatives of the momentum equation near the equator. In this study, we apply the method of Vianna and Menezes [2003] for velocity calculations within ± 3° off the equator.

The a priori errors involved in the our methodology of geostrophic velocity estimation, which uses horizontal gradients of DH, are due to temperature precision of ± 0.1°C in the XBT measurements (O[1 cm/s]); salinity estimates from the T-S relationship (O[5 cm/s]); uncertainty in the level of known motion (O[1 cm/s]); and the angle of the transect with the true meridional (O[4 cm/s]) or smaller than 10% error in the region (Reverdin et al., 1991), assuming a priori small zonal pressure gradients. These errors add up to ± 11 cm/s, which is the order or smaller than the intrinsic mesoscale variability of the region. Therefore the standard monthly error will be used as a confidence interval for our calculations. At the equator, the beta plane approximation generates errors one order of magnitude greater (O[10 cm/s]) than the other components, and this caveat has to be taken into consideration in our analysis.

Synthetic method

Altimetry can be used along with other observational platforms to provide a broader four dimensional (spatial and temporal) coverage of the tropical Atlantic. Several works have used altimetric and hydrographic data to infer properties of the upper ocean, such as velocity, temperature, and salinity [e.g., Gilson et al., 1998; Ridgway, 2002; Phillips and Rintoul, 2002; Carnes et al., 1990].

Here, we apply a synthetic method to produce a hindcast of the velocity and density fields along the mean AX08 transect position (red line in Figure 1c). Since we are interested in velocity sections along isopycnal layers, we use as predictands potential density (σ_θ) and dynamic (steric) height (DH) from the surface to 800 m. The synthetic method uses altimetric information of sea surface height anomalies to generate the predictors. For this, we first calculate the absolute DH (Equation 1) for the 32 selected XBT sections. Anomalies of σ_θ and DH (σ'_θ and DH', respectively) are calculated by subtracting one mean annual field, defined by the mean WOD01 density field along the mean section, and the mean dynamic height of all sections. For the latter, we first calculate monthly averages to reduce potential sampling biases towards any specific month. These results are mostly insensitive to the mean fields, since they just subtract a constant from the temporal fields, but subtracting a mean is known to reduce the variance of residuals in a linear regression. Anomalies of surface DH (DH'_0) are linearly regressed onto DH' and σ'_θ as a function of location and depth. Finally, the DH'_0 is linearly regressed onto SSA, thus forming the link between the satellite and hydrographic observations. The DH'_0 and SSA are well correlated (Figure 5), with an R-squared coefficient $R^2 = 0.72$, which is equal to the squared correlation in a simple linear regression, and a negligible intercept. This strong and unbiased relationship between the two variables show that the SSA captures well the baroclinic structures in the region, in specially the first mode. The highest variance of SSA occurs between 5-10°N, in the same region where the highest SSH gradients are located, and which are closely related to the dynamics of the NECC. Less variability is seen south of the equator, which can be due to compensating effects in the water column [Mayer et al., 2001]. The differences found here between SSA and DH'_0 can arise from a number of factors, such as temporal and spatial sampling, tides not completely removed, as well as variations in the barotropic flow and changes in the entire depth of the ocean [Rintoul et al., 2002].

One indicator of the skill of this method to monitor the variability of the predictands DH' and σ'_θ is the temporal correlation between DH'_0 and the predictands at each depth and latitude. The correlations (Figure 6) exhibit, as expected, opposite signs for DH' and σ'_θ, since dynamic height is calculated from steric volume anomalies, which are inversely related to density [Pond and Pickard, 1983]. Apart from their sign, both fields show similar relationships, with highest correlations in the upper 200 m of the water column, and decreasing magnitude with depth. In certain latitudes, such as around 5°N, high correlations ($R > 0.8$) can reach depths of 800 m, similarly to features described in Roemmich and Gilson [2001].

3. Results

The central tropical Atlantic has a very characteristic seasonal variability of the surface dynamic height. December through May are characterized by an almost flat DH_0 between 10°S-10°N, implying small surface geostrophic velocities (Figure 3a,b). From June through November (Figure 3c,d) there is a stronger gradient of DH_0 north of 5°N, and the NECC core is well defined. A double NECC core is developed seasonally around 8°N, especially during the boreal fall, which is merged back into one single and stronger core generally during late summer/early fall. There is often a connection between the surface NECC with the thermocline layer, and the NEUC can be found as a lobe attached to the NECC. Two cores are also found in the thermocline layer in the north of the section, and the northernmost one is referred as the northern NECC core (nNECC; e.g., Didden and Schott [1992], Urbano et al. [2006]). During the spring, however, the NEUC is clearly detached from the nNECC. The isopycnic signature of the NEUC on the σ_θ = 26.5 isopycnal is seen at about 5°N, but does not show a very sharp gradient [c.f., Bourles et al, 2002; Schott et al., 2003]. In contrast, the isopycnic signature in the south around 4-5°S, where the SEUC is located around 200 m, has a very distinguished southward elevation of the σ_θ = 26.5 isopycnal. This is an indication that the meridional pressure gradient is a major driver of the SEUC variability. The isopycnal signature of the SEUC and its well defined core are visible throughout the year; therefore the SEUC is a permanent feature in the tropical Atlantic. The EUC core is located mostly south of the equator, and its core is generally located between the surface and 100 meters.

We define the location of the equatorial eastward currents by assigning a latitudinal band to each of the currents (Figure 3), similarly to Hüttl-Kabus and Böning [2008]: the NECC is defined between 3°-10°N; the NEUC between 3°-6°N; the SEUC between 3°-6°S; and the EUC between 2.5°S and 2.5°N. We further characterize these currents by selecting isopycnal layers to define their vertical boundaries: one upper or surface layer, from the surface to σ_θ =24.5 kg m^{-3}, and one lower or thermocline layer, from σ_θ =24.5 - 26.8 kg m^{-3} [Schott et al. 1998]. The upper layer contains the NECC and part of the EUC, and the lower layer comprises OEUCs and deeper contribution of the EUC.

Synthetic method validation

We validate the synthetic method by comparing the transports of the eastward equatorial currents estimated from the 32 XBT transect realizations with their synthetic estimates along the same sections (Figure 7). The agreement between the transport estimated synthetically and from hydrography is high for the NECC (Figure 7a, b). The transport differences are in general less than 1 Sv, and in most of the cases the values are coincident with each other. A strong linear relationship is found between the two estimates, with the corresponding R^2 = 0.95 for the linear fit. The EUC (Figure 7g, h), which has transport contributions from the upper and lower layers, and also accounts for artifacts of the equatorial beta approximation, shows a moderate-to-high agreement between the two estimates (R^2 = 0.55).

Regarding the OEUCs, the synthetic method has still some skill for the NEUC (R^2 = 0.33), but the transports using XBT data are generally higher than the synthetic ones (Figure 7c, d). The method fails for the SEUC, and the variance of the synthetically-derived SEUC transports barely resemble the ones from hydrography (Figure 7e). However, a mean transport of around 7 Sv is found on both methods. Due to the low agreement between the two SEUC transport estimates, the analysis of the synthetic method will only be applied to the EUC, NEUC and NECC.

3.1 Seasonal variability

Here we analyze the seasonal variability of the NECC, SEUC, NEUC and EUC along the AX08 transect in terms of across transect transport, location and velocity at the core, using for this monthly averages of these variables. The selected 32 sections provide high resolution coverage along the central Atlantic of all months except February (Figure 1b). We apply the method of Foltz et al. [2004a] to the XBT-derived quantities to estimate the monthly mean and variance of transport, core velocity and position of the currents. This method fits the first two harmonics (annual and semi-annual) to the data in a least square fashion. It accounts for observational uncertainties by calculating a diagonal covariance matrix, with each diagonal term corresponding to a month, calculated as the sum of the fitting residual error and the observational error given by the standard deviation of each month. Fitting the first two annual harmonics to the data filter a large part of the mesoscale features. Below we analyze the each of the currents separately.

a) NECC

The hydrographic data estimates show a strong annual cycle of the NECC, which alone represents 61% of the total transport variance, 34% of the maximum velocity and 50% of position variances (Table 1). Earlier analyses from drifter data also show a dominant contribution as high as 80% of the annual cycle for off-equatorial surface currents [e.g., Richardson and Walsh, 1986]. The NECC reaches its southernmost position in April-May (~3-4°N), concomitant with its lowest transport (~1 Sv), and its northernmost position (~7-9°N) in September-October (Figure 8i), at the period of its highest transport (~10-11 Sv) reached during summer/fall (Figure 8a). This seasonal variability of the NECC agrees with previous observational findings [Richardson et al., 1992], and is known to be linked to the north-south migration of the ITCZ [Katz and Garzoli, 1982; Katz, 1987; Garzoli and Richardson, 1989; Garzoli, 1992], which is near the equator during boreal spring and farthest north during boreal summer. The NECC core velocity shows a similar pattern, with lowest values (~10-20 cm/s) in boreal spring and maximum values (~55 cm/s) in boreal fall (Figure 8e).

The synthetic estimates for the comparable 2000-2010 period, given by the blue line in Figure (8a,e,i), follow closely the ones from hydrography. As the synthetic estimates are averaged using a much longer time series, and the hydrographic data is subject to higher influence of mesoscale effects due to sparse temporal sampling (Figure 1b), differences are expected. For instance, the synthetic method shows generally higher explained variance for the annual cycle, from 78-92% of the transport variability. Regarding the maximum velocity time series (Figure 8e), the synthetic estimates show strong semi-annual variability (blue and green curves) that is not obvious in the hydrographic data (red curve). Our results suggest that, when comparing the synthetic estimates from the 2000-2010 decade to the ones from the previous decade (1993-2000), there is an increase in the transport of the NECC of about 1-2 Sv (Figure 8a). This change is however in the range of difference between the XBT and synthetic estimates.

The characteristics of the NECC transport over time can be retrieved by applying a wavelet transformation onto the NECC transport timeseries for the whole altimetric period (Figure 9a). The wavelet analysis [Torrence and Compo, 1998] confirms that the annual cycle of the NECC is the strongest signal. Furthermore, the energy of the annual period seems to be enhanced since 2002, in agreement with the transport increase in the climatological time series (Figure 8a). The mechanisms related to interannual variability of this current, as well as for the NEUC, are explored in the section 3.2.

b) SEUC

The XBT-derived transport of the SEUC (Figure 8c) is weaker (~6 Sv) from July to September, in agreement with Reverdin et al. [1991], and also reduced in January-February (~5 Sv). Maximum transport values are found from October through December, reaching over 10 Sv, and the mean SEUC transport is about 7-8 Sv, in close agreement with Brandt et al. [2006] and Fisher et al. [2008]. The semi-annual harmonic is dominant, and explained variances are 90% for transport and 90%for maximum velocity, in agreement with the model work of Hüttl-Kabus and Böning [2008]. The core velocity is about 28 cm/s in May/June and October, and 20 cm/s in August (Figure 8g). Fisher et al. [2008] estimates a weaker mean SEUC velocity of 17.9-13.4 cm/s in the region comprehending 23°W, but departures from this mean were found to add up to 50 cm/s in its core. The mean position of the SEUC is about 4.5±0.5°S, and its position variability follows closely its transport variability, in that higher transports are associated to a more northern position and vice versa.

c) NEUC

The NEUC shows higher transport values during boreal spring (Figure 8b), when its transport ranges from 5-10 Sv, and low transports (~3 Sv) are observed in boreal fall. In comparison to the NECC transport seasonal cycle (Figure 8a), the NEUC bears an almost inverse relationship with the NECC, and therefore with the location of the ITCZ. The annual cycle dominates the XBT transport variability (54% of variance), whereas the semi-annual cycle only explains 1% of variance. The NEUC location (Figure 8i) cycle resembles the transport one, with more southward position (~3.5-4°N) in the boreal spring at the time of higher transport. The NEUC core velocity (Figure 8f) is mostly semi-annual (49% of variance), with core speed of about 25 cm/s in boreal winter/summer, and smaller core velocity of about 10-15 cm/s during September-October, revealing that the NEUC is still present during these months. Synthetic estimates broadly agree in magnitude with the XBT ones, and may show some changes between the 1990's and 2000's decades. The wavelet analysis of the whole altimetric period indicates a possible shift in energy from a prevailing semi-annual to an annual variability starting in 2000 (Figure 9b). This energy peak is related to mesoscale features and wave mechanisms that are integral part of the NEUC dynamics. There is a hint of interannual variability in the NEUC transport, with increased energy centered in 1995, 2000 and 2006. The resemblance between the variability of the zonal winds in the equatorial region (Figure 9d) and the NEUC transport variability is notorious. Possible dynamical mechanisms of the NEUC variability will be explored in the next section.

d) EUC

Both methods agree well in that the EUC at 23°W is mostly located south of the equator, between -1±1°S (Figure 8l). Despite the fact that the seasonal variability of the position of the EUC is small, there is indication of a more southward position is during late boreal fall/winter. The core velocity from XBT agrees reasonably well with the synthetic method, but higher range, from 20-45 cm/s for XBT estimate, and 20-30cm/s for the synthetic estimate. These values are somewhat smaller than direct velocity observations of the EUC, which show higher values (~80-

90 cm/s) in the EUC core [Giarolla et al., 2005; Brandt et al., 2006, 2008]. The EUC transport hinges to a semi-annual variability from both hydrographic and synthetic estimates (Figure 8d), with lower values during the summer and winter, and higher values during spring and late summer-early fall. The wavelet analysis (Figure 9c) confirm the observed findings of a strong semi-annual transport variability of the EUC, in agreement with results from previous model studies for the central equatorial Atlantic [Arhan et al., 2006; Hormann and Brandt, 2007; Kolodziejczyk et al., 2009]. The high variability of the XBT estimates in some months, see for instance the errorbars of transport and core velocity during July (Figures 8d,h), are artifact of the performance of the equatorial method for specific density structure of the month, and need to be interpreted carefully.

3.2 Interannual variability

In this section, we investigate statistically the interannual signature of the NECC and NEUC on the sea surface temperature (SST) and surface wind stress. We restrict our analysis to the NECC and NEUC transports only because the synthetic method does not provide good estimates of the SEUC variability, and we do not expect that the equatorial beta approximation can produce reliable estimates of the EUC transport variability on interannual timescales. We use in this analysis monthly transport anomalies with respect to their monthly climatology, with the intent of reducing the influence of eddy variability on these currents. Furthermore, we perform a correlation analyses of the monthly transport anomalies of the NECC and NEUC with both the gridded monthly anomalies of SST [Reynolds et al., 2002] and pseudo-wind stress (CCMP; Atlas et al. [1996]) datasets. Correlations are performed for the 1993-2011 period over the tropical Atlantic, taking only statistically significant values into account ($p < 0.05$). In this analysis, all data are standardized by subtracting their mean and dividing by their standard deviation, and smoothed with a 5-month moving average.

a) NECC

The correlation of the NECC transport anomalies with SST anomalies (SSTA) for the altimetric period produces a very distinctive pattern in the form of an anomalous interhemispheric SST gradient (Figure 10), with positive phase north, just off equator in the ITCZ region, centered at ~30°W/2°N and extending northeastward, and negative phase in the central south of the domain, with center at ~20°S/17°W. The corresponding correlation with pseudo-wind stress anomalies indicates an anomalous strengthening of the southeasterly trade winds, with largest magnitude in the western equatorial region, where winds are also strongest. This pattern is reminiscent of the meridional mode and agrees with an underlying mechanism explained by the wind-evaporation-SST (WES) feedback, which involves interactions between SST changes and wind-induced latent heat flux [Xie and Philander, 1994; Chang et al., 1997]. Similar pattern has been also found for the NECC in a recent study using CEOF analysis surface drifter data [Hormann et al., 2012].

The SSTA gradient index can be defined by subtracting area averages of positive (35°W-17°W/0°-7°N) and the negative (30°W-15°W/11°S-23°S) correlation regions. The correlation between the monthly NECC transport anomalies and the SST index is $R=0.45$, with maximum correlation at zero lag. The meridional wind (y-wind) index that is centered in the northern box above described, which focus on the variability of the meridional wind stress near the central equatorial region, shows a positive correlation of also R=0.45, with the NECC leading the wind strengthening within one month lag. This relationship indicates that there is a fast response of the NECC to temperature and wind anomalies that might be explained by either the fast adjustment time of the ocean through equatorial waves [e.g., Ma, 1996] or with anomalies connected with the simply strengthening of the surface retroflection of the NBC.

b) NEUC

For the NEUC transport anomalies, the pattern arising from its correlation with SST and wind stress anomalies (Figure 11) can be described as follows: while negative SST coefficients prevail in the northeastern part of the basin, positive correlations are found along the equator and on the southwestern African coast, in addition to reduced trades in the western to central equatorial Atlantic. These two regions of high interannual SST variability are sites where the thermocline is rather shallow, in which anomalous SSTs are highly correlated with thermocline depths [Carton et al., 1996], and therefore are closely linked to the equatorial mode [Zebiak, 1993]. Some studies [c.f, Chiang et al., 2001; Foltz et al., 2011] define the difference of anomalous SST averaged within these two regions as the Atlantic Meridional Mode (AMM). This pattern is tied to the seasonal cycle [Servain et al., 1999], in which anomalous negative/positive SST gradient in boreal spring is associated with westerly/easterly equatorial wind anomalies. Therefore, winds at the equatorial region respond to this negative pattern of the interhemispheric SST gradient by reducing their strength, therefore shifting the ITCZ south [Moura and Shukla, 1996]. This could reinforce the positive anomaly in the equatorial region by decreasing upwelling there [Foltz et al., 2011]. Similar pattern was also found in model studies for the upwelling regions of virtual lagrangian floats released inside the NEUC [Stramma et al., 2005; Huettl-Kabus and Boening, 2008]. Therefore a relationship between the overlying atmospheric variability and the NEUC dynamics can be drawn, taking into account the current knowledge of the variability of the region. According to the model study of Huettl-Kabus and Boening [2008], part of the NEUC can merge on the EUC, contributing for the equatorial upwelling. Since the EUC and NEUC are known to pertain to only one core at their origin in the western Atlantic, their synergy with respect to the equatorial upwelling may be expected. In addition, Stramma et al. [2005] shows a direct trajectory from virtual lagrangian particles from the NEUC towards the Guinea Dome. Some mechanisms have been proposed to describe the link between these two regions of high SST variability [e.g., Doi et al., 2009], in which both coastal upwelling in the Guinea Dome and WES feedback related to the Atlantic meridional mode are involved. In the Guinea Dome region, where the NEUC transport is negatively correlated with SSTA, prevailing wind anomalies are directed to the southwest, proper for the increased coastal upwelling in the region. This link between the NEUC and the Guinea Dome has long been proposed [e.g., Voituriez, 1981], since the uplifting of the thermal structure in the dome extends much further down the thermocline. The strong upwelling in the region is related, for instance, to the outcropping of the σ_θ = 24.5 layer. The dynamics underlying this relationship is that a cooler Guine Dome and warmer equatorial region would increase the north-south density gradient in the NEUC region, and strengthen its core. Some studies indeed suggest that the upwelling in the Guinea Dome region can drive the NEUC variability [MCready et al., 2002]. Likewise we have produced for the NECC analysis, we create one interhemispheric SST index, now taking into account the difference between the SSTA in the Guinea Dome region (15°-25°N/15°-30°W) and in the southeast Atlantic (0-8°S/15°W-10°E), along with one meridional wind stress index inside the Guinea Dome box. The correlation between the NEUC transport and the SST index is R = -0.50 at zero lag, and R = -0.31 with the y-wind index in the Guinea Dome. This significant link between the variability of the AMM and the equatorial mode with the NEUC might explain the interannual pattern observed in the wavelet analysis (Figure 9b), such that the anomalously strong SST gradient during 1and increased Guinea Dome upwelling strengthened the NEUC during those periods.

4. Discussion and Conclusions

In the present study, we use a combination of HD XBT transect data along with altimetry to investigate the variability of the eastward surface and subsurface currents in the equatorial Atlantic. The AX08 XBT transect is carried out on average four times a year since 2000. The high spatial resolution of the hydrographic data and its repeated sampling rate of the region enable us to assess the dynamical and thermodynamical properties of the upper ocean, and permit the characterization of the seasonal cycle of major geostrophic zonal currents, such as the NECC and NEUC. However, due to strong intra-seasonal variability generated by the eddy variability and the passage of TIWs in the region [Weisberg and Weingartner, 1988; Jochum et al., 2004], it is necessary to carry out a high number of sections for one to be able to produce a good statistical estimate of the seasonal cycle of these currents using hydrography only. For instance, from the 32 XBT sections analyzed, observations during the months of January, May and June were only carried once in each month, and there is yet no section available for February.

Merging altimetry and XBT data with this synthetic methodology reproduces the main features of the transect with depth that cannot be seen with altimetry alone, and overcome the sampling restriction and produce a smoother estimate of the long term average of the properties of the currents. The best performance of the synthetic profile methodology for the AX08 region resides in the upper 200-300 m of the water column, where the temporal correlations of SSA and anomalies of density and dynamic height are above 0.8.

The seasonal cycle of the eastward equatorial currents derived from our analyses are in good agreement with previous works [e.g., Peterson and Stramma, 1990; Bourles et al., 2002]. The NECC contains a strong seasonal cycle, with transport ranging from 1 to 11 Sv and maximum speed greater than 50 cm/s. Its seasonal variability is related to the migration of the ITCZ (not shown), with stronger transport positively correlated to the northward shift of the ITCZ. On interannual timescales, the NECC strength is linked to the strengthening of the southwesterly trade winds and an interhemispheric SST gradient pattern (positive north and negative south). The NECC strengthening during positive interhemispheric SST gradient might act as a positive feedback, since it would increase the eastward transport of warmer western waters in the region of the SST maximum gradient. This SST pattern is known to be influenced by the Atlantic Meridional Oscillation (AMO), and North Atlantic Oscillation (NAO), and connections from the eastern Pacific [Enfield and Mayer, 1996] There is indication of a recent strengthening of the climatological NECC of ~1-2 Sv, and attribution can be related to the recent decrease in sulphate aerosols emissions over the North Atlantic, and the associated increase in the SST there and consequent trend northward of the ITCZ [Chang et al., 2011].

The NEUC annual cycle is characterized by stronger transport values from January-July up to 10 Sv, therefore in opposite phase to the NECC transport cycle. The NEUCs core is located between 4-6°N with maximum velocities of about 30 cm/s in June-July. Synthetic estimates suggest that the semi-annual range of the spectrum used to be stronger during the 1990's, and that there was a shift to a more annual period, which shows to be intermittent, since 2000. This agrees with the pattern variability of the Atlantic meridional mode (AMM) described in Foltz et al. [2011]. We show that the variability of the NEUC transport is statistically related to the upwelling in the AMM and the variability Guinea Dome region [Schott et al. 2004].

NEUC and NECC bear an inverse relationship of transport in interannual timescales. Both are linked to the variability of the cross equatorial wind stress, but the NECC has positive values for increased southwesterlies whereas the NEUC is increased to negative southwesterlies anomalies. The interannual modes of tropical Atlantic variability are strongly tied to their seasonal cycle [Nobre and Shukla, 1996], therefore this also explains the inverse relationship between NEUC and NECC that holds for seasonal timescales.

The SEUC calculated from hydrography is located on average at 4.5°S, and presents a weaker seasonal cycle, with mean transport of about 8 Sv, higher values from October-December, and a secondary peak during May-June. Velocities during the stronger months range from 25-30 cm/s. The synthetic method so far represented well the mean flow but not its variability. This may be a shortfall of our methodology since the variability of SSA in the southern tropical Atlantic is somewhat weak (Figure 1c), and the surface signature of the current is masked by compensating effects in the water column (Figure 6). The compensating effects can be, for example, driven by buoyancy and wind forcing components of the same magnitude and with opposing signals [Mayer et al., 2001]. Therefore, a regular sampling from the HR XBT transect is particularly important for monitoring the SEUC.

The EUC can be resolved by the equatorial beta approximation using hydrographic data. The EUC seasonal cycle is well explained using the first and second harmonics, with peaks in boreal fall and boreal spring, therefore the semi-annual period is important for its variability in the region. The mean EUC transport is around 15 Sv, close to direct observations [e.g., Brandt et al., 2006], but the maximum velocity at the core ranges within 30-40 cm/s, about 50 % of direct mooring observations [e.g., Giarolla et al., 2005], which is a known artifact of the equatorial beta plane approximation [e.g., Langerlof et al., 2000]. A comparison with EUC transport estimates using mooring data in the equatorial region (Andreas Funk, personal communication) shows similar annual variability as the one derived from the method of Vianna and Menezes [2003].

Results from this study are subject to specific caveats that provide avenues for future studies and improvements to the methodology. First, we use a simple statistical method to infer relationship between the surface height and the ocean properties at depth. Using an improved statistical method may allow the inclusion of additional information, such as latitudinal cross-correlation between and autocorrelation of the residuals with depth, and use if additional constraints derived from co-located observations. Second, we use climatological values of salinity calculated from the mean T-S relationship at each location, and also climatological values of the absolute dynamic height at 800 m. Available observations from ARGO, for example, could reduce errors in the methodology. However, these observations are mostly restricted to the last 5-6 years. Third, along track data might provide better agreement between altimetric sea surface height and hydrographic-based dynamic height at the surface, since it is less smoothed by optimal interpolation procedures. Finally, high resolution modeling can fill the gaps of the observational results, and confirm if our conclusions in a dynamically consistent fashion. These possibilities will be explored in a future study.

Acknowledgements

The authors would like to thank Greg Foltz and Rick Lumpkin for insightful discussions. This research was carried out under the auspices of the Cooperative Institute for Marine and Atmospheric Studies (CIMAS), a cooperative institute of the University of Miami and the National Oceanic and Atmospheric Administration, cooperative agreement #NA17RJ1226. Any errors and opinions are those of the authors alone.

References

Atlas, R., R. N. Hoffman, S. C. Bloom, J. C. Jusem, and J. Ardizzone (1996), A multiyear global surface wind velocity data set using SSM/I wind observations. Bull. Amer. Meteor. Soc., 77, 869–882.

Bourles, B., Y. Gouriou, and R. Chuchla (1999), On the circulation in the upper layer of the western equatorial Atlantic, J. Geophys. Res., 104, C9, 21.151-21.170.

Bourles, B., M. D’Orgeville, G. Eldin, Y. Gouriou, R. Chuchla, Y. DuPenhoat, and S. Arnault (2002), On the evolution of the thermocline and subthermocline eastward currents in the Equatorial Atlantic, Geophys. Res. Lett., 29(16), 1785, doi: 10.1029/2002GL015098.

Brandt, P., V. Hormann, B. Bourle`s, J. Fischer, F. A. Schott, L. Stramma, and M. Dengler (2008), Oxygen tongues and zonal currents in the equatorial Atlantic, J. Geophys. Res., 113, C04012, doi:10.1029/2007JC004435.

Chang, C-Y, J.C.H. Chang, M.F. Wehner, A.R. Friedman and R. Ruedy (2011), Sulfate Aerosol Control of Tropical Atlantic Climate over the Twentieth Century, J. Climate, 24, 2540-2555, DOI: 10.1175/2010JCLI4065.1.

Cheney, R., L. Miller, R. Agreen, N. Doyle and J. Lillibridge (1994), TOPEX/Poseidon: The 2-cm solution, J. Geophys. Res., 99, 24,555-24,563.

Conkright, M. E., et al. (2002), World Ocean Database 2001, vol. 1, Introduction, NOAA Atlas NESDIS 42, 159 pp., U.S. Gov. Print. Off., Washington D. C.

Didden, N., F. Schott (1992), Seasonal variations in the Western Tropical Atlantic: surface circulation from geosat altimetry and WOCE model results. J. Geophys. Res. C 97 (3), 3529–3541.

Ducet, N., P.-Y. Le Traon, and G. Reverdin (2000), Global high resolution mapping of ocean circulation from Topex/Poseidon and ERS-1 and -2, J. Geophys. Res., 105 (C8), 19477-19498.

Fischer, J., V. Hormann, P. Brandt, F. A. Schott, B. Rabe, and A. Funk (2008), South Equatorial Undercurrent in the western to central tropical Atlantic, 35, L21601, doi: 10.1029/2008GL035753.

Foltz, G., S. Grodsky, and J. Carton (2004a), Seasonal salt budget of the northern tropical Atlantic Ocean along 38°W, J. Geophys. Res., 109, C03052, doi: 10.1029/2003JC002111.

Foltz, G., J. Carton, E.P. Chassignet (2004b), Tropical instability vortices in the Atlantic Ocean, J. Geophys. Res., 109, C03029, doi: 10.1029/2003JC001942.

Fonseca, C., G. Goni, W. E. Johns, and E. J. D. Campos (2004), Investigations of the North Brazil Current retroflection and North Equatorial Countercurrent variability, Geophys. Res. Lett., 31, L21304, doi: 10.1029/2004GL020054.

Frantantoni, D., W. E. Johns, T. L. Townsend, and H. E. Hurlburt (2000), Low latitude circulation and mass transport pathways in a model of the tropical Atlantic Ocean. J. Phys. Oceanogr., 30, 1944–1966.

Goes, M., and I. Wainer (2003), Equatorial Currents transport changes for extreme warm and cold events in the Atlantic Ocean, Geophys. Res. Lett., 30 (5), doi: 10.1029/2002GL015707.

Goes, M., R. Molinari, I. C. A. Silveira, and I. Wainer (2005), Retroflections of the North Brazil Current during February 2002. Deep Sea Research Part 1. Oceanographic Research Papers, v. 52, n. 3, pp. 647-667, doi: 10.1016/j.dsr.2004.10.010.

Goldenberg, S. B., C. Landsea, A. M. Mestas-Nunez, and W. M. Gray (2001), The recent increase in Atlantic hurricane activity, Science, 293, 474– 479.

Hüttl-Kabus, S., and C. W. Böning (2008), Pathways and variability of the off-equatorial undercurrents in the Atlantic Ocean Journal of Geophysical Research - Oceans, 113. C10018. ISSN 0148-0227. DOI: 10.1029/2007JC004700.

Jochum, M., P. Malanotte-Rizzoli, and A. Busalacchi (2004a), Tropical instability waves in the Atlantic Ocean, Ocean Modell., 7, 146–163.

Jochum, M., and P. Malanotte-Rizzoli (2004), A new theory for the generation of the equatorial subsurface undercurrents, J. Phys. Oceanogr., 34, 755–771.

Lagerloef, G., G. T. Mitchum, R. B. Lukas, and P. Niiler (1999), Tropical Pacific near surface currents estimated from altimeter, wind and drifter data, J. Geophys. Res., 104, 23,313-23,326.

Le Traon P.Y., F. Nadal, N. Ducet (1998), An improved mapping method of multisatellite altimeter data. J. Atmos. Oceanic Technol., 15, 522-533.

Locarnini, R. A., A. V. Mishonov, J. I. Antonov, T. P. Boyer, and H. E. Garcia (2006), World Ocean Atlas 2005, Volume 1: Temperature. S. Levitus, Ed. NOAA Atlas NESDIS 61, U.S. Government Printing Office, Washington, D.C., 182 pp.

Mayer, D., R.L. Molinari, and M. O. Baringer (2001), Transition regions and their role in the relationship between sea surface height and subsurface temperature structure in the Atlantic Ocean, Geophysical Research Letters, 28, 20, 3943-3946.

McCreary, J.P., P. Lu, and Z. Yu (2002), Dynamics of the Pacific subsurface countercurrents. J. Phys. Oceanogr., 32, 2379–2404.

Nobre, P., and J. Shukla (1996), Variations of sea surface temperature, wind stress and rainfall over the tropical Atlantic and South America, J. Clim., 9, 2464– 2479.

Picaut, J., and R. Tournier (1991), Monitoring the 1979-1985 equatorial Pacific current transports with expendable bathythermograph data, J. Geophys. Res., 96, 3263-3277.

Pond, S. and G. Pickard (1983), Introductory Dynamical Oceanography, 2nd Ed., Pergamon Press Inc., NY 10523, USA.

Reverdin, G., P. Rual, Y. du Penhoat, and Y. Gouriou (1991), Vertical structure of the seasonal cycle in the central equatorial Atlantic Ocean: XBT sections from 1980 to 1988, J. Phys. Oceanogr., 21, 277-291.

Reynolds, R.W., N.A. Rayner, T.M. Smith, D.C. Stokes, and W. Wang (2002), An improved in situ and satellite SST analysis for climate. J. Climate, 15, 1609-1625.

Richardson, P.L., and D. Walsh (1986), Mapping climatological seasonal variations of surface currents in the tropical Atlantic using ship drifts, Journal of Geophysical Research, 91, 10537-10550.

Ridgway, K. R., R. C. Coleman, R. J. Bailey, and P. Sutton (2008), Decadal variability of East Australian Current transport inferred from repeated high-density XBT transects, a CTD survey and satellite altimetry, , J. Geophys. Res., 113, C08039, doi:10.1029/2007JC004664.

Rintoul, S. R., S. Sokolov, and J. Church (2002), A 6 year record of baroclinic transport variability of the Antarctic Circumpolar Current at 140°E derived from expendable bathythermograph and altimeter measurements, J. Geophys. Res., 107(C10), 3155, doi:10.1029/2001JC000787.

Rio, M. H., S. Guinehut, and G. Larnicol (2011), New CNES-CLS09 global mean dynamic topography computed from the combination of GRACE data, altimetry, and in situ measurements, J. Geophys. Res., 116, C07018, doi:10.1029/2010JC006505.

Roemmich, D., J. Gilson (2001), Eddy Transport of Heat and Thermocline Waters in the North Pacific: A Key to Interannual/Decadal Climate Variability? J. Phys. Oceanogr., 31, 675–687.

Schott, F., L. Stramma and J. Fischer (1995), The warm water inflow into the western tropical Atlantic boundary regime, spring 1994, Journal of Geophysical Research 100, pp. 24745–24760.

Schott, F., J. Fisher, and L. Stramma (1998), Transports and pathways of the upper-layer circulation in the western tropical Atlantic, Journal of Physical Oceanography, 28, pp. 1904–1928.

Schott, F. A., M. Dengler, P. Brandt, K. Affler, J. Fischer, B. Bourles, Y. Gouriou, R. L. Molinari, and M. Rhein (2003), The zonal currents and transports at 35°W in the tropical Atlantic, Geophys. Res. Lett., 30, 7, 1349, doi:10.1029/2002GL016849.

Sutton, R. T. and Hodson, D. L. R. (2005), Atlantic Ocean forcing of North American and European summer climate. Science, 309 (5731), 115-118, doi: 10.1175/JCLI4038.1.

Torrence, C and G. P. Compo (1998), A Practical Guide to Wavelet Analysis., Bulletin of the American Meteorological Society, 79, 1, 61-78. Software available at URL: http://atoc.colorado.edu/research/wavelets/

Urbano, D. F., M. Jochum, and I. C. A. Silveira (2006), Rediscovering the second core of the Atlantic NECC, Ocean Modell.,12, 1–15,doi:10.1016/j.ocemod.2005.04.003.

Vianna, M., and V. V. Menezes (2003), A seasonal and interannual study of the western equatorial Atlantic upper thermocline circulation variability, In: Interhemispheric Water Exchange in the Atlantic Ocean, G.Goni & P.Malanotte-Rizzoli, Editors, 2003: 137-174.

Voituriez, B. (1981), Les sous courants equatoriaux Nord et Sud et la Formation des domes thermiques tropicaux, Oceanolog. Acta., 5, 497-506.

Weisberg, R., and T. Weingartner (1988), Instability waves in the equatorial Atlantic Ocean, J. Phys. Oceanogr., 18, 1641– 1657.

Figures:

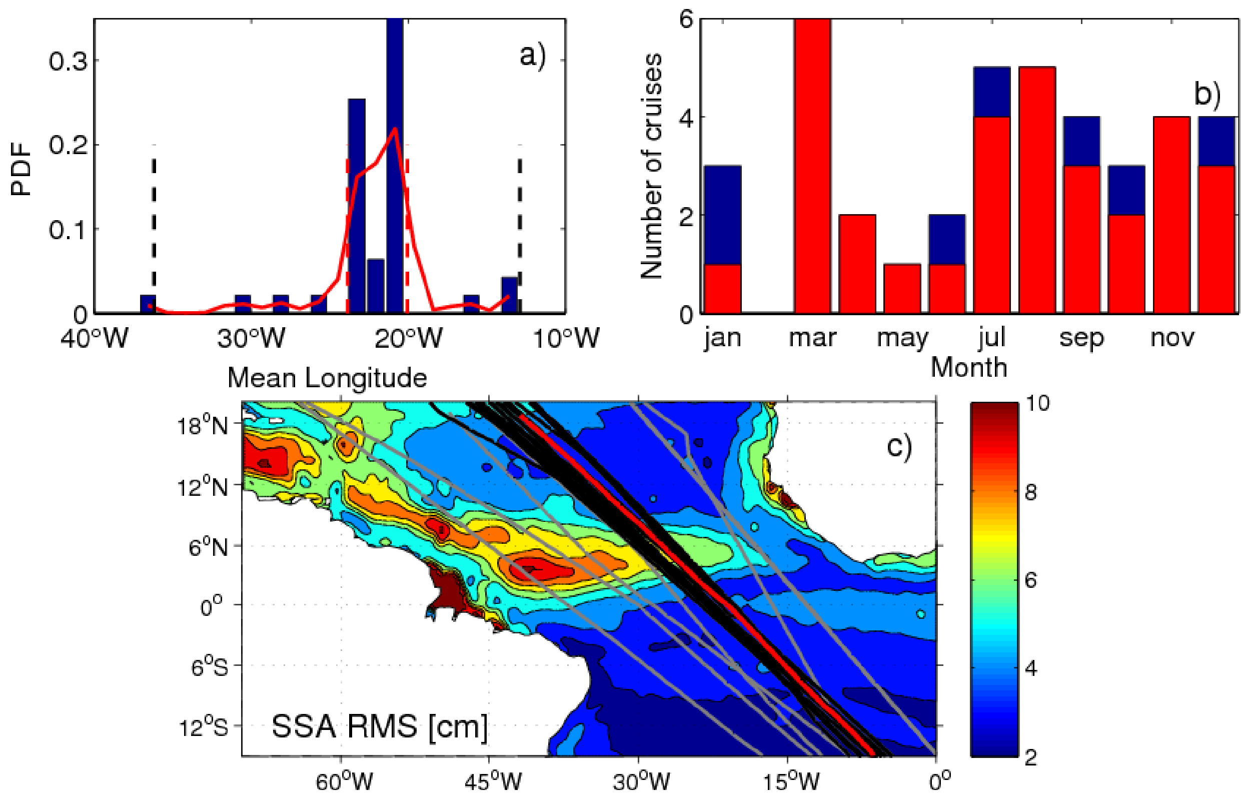

Figure 1: a) Probability density function of the averaged longitude between 10°S-10°N for all the AX08 XBT sections. b) Histogram of the monthly distribution of the number of the sections before (blue) and after (red) the selection of the sections that fit into the 68 percentile of a). c) Root mean square of SSA (cm) in the tropical Atlantic (filled contours), with superimposed AX08 sections: selected sections (black), sections not included in the analysis (gray), and mean of the selected sections (red).

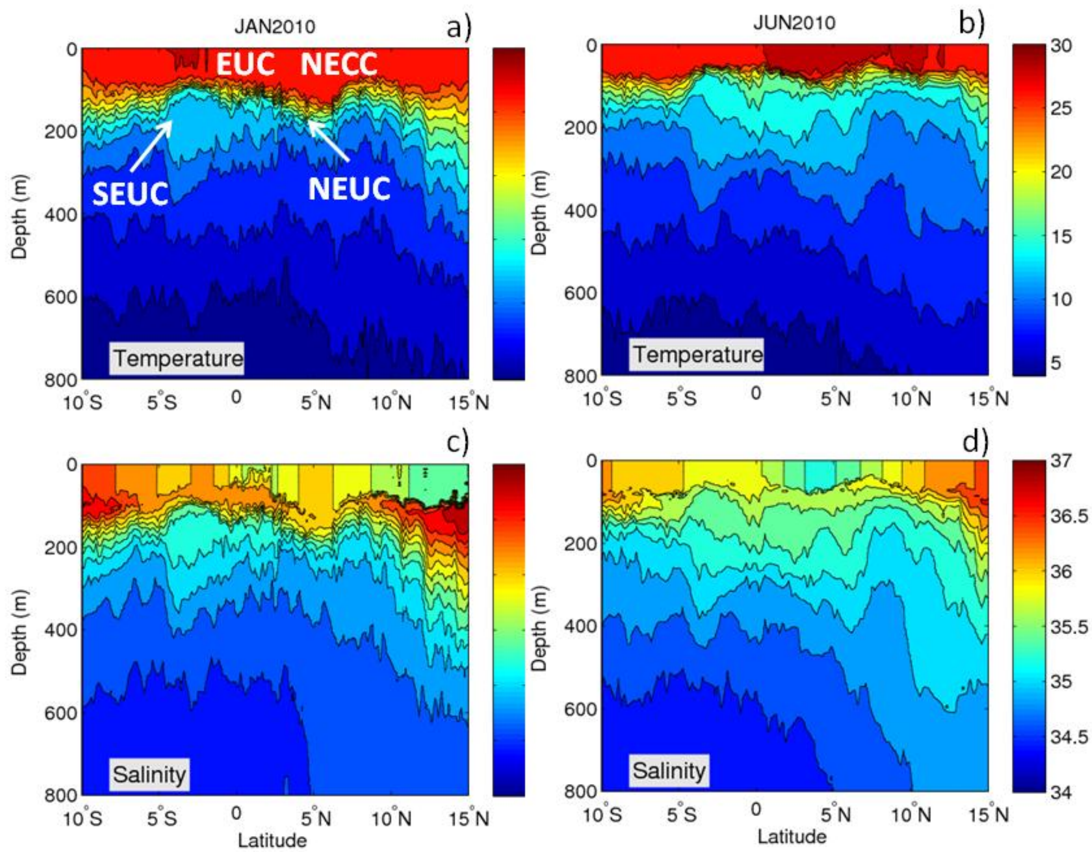

Figure 2: Example of typical temperature (°C) and salinity (psu) sections for January 2010 (left) and June (right). Salinity is derived from the mean T-S relationship using WOD01. The name of the eastward currents are written over their mean positions in panel (a).

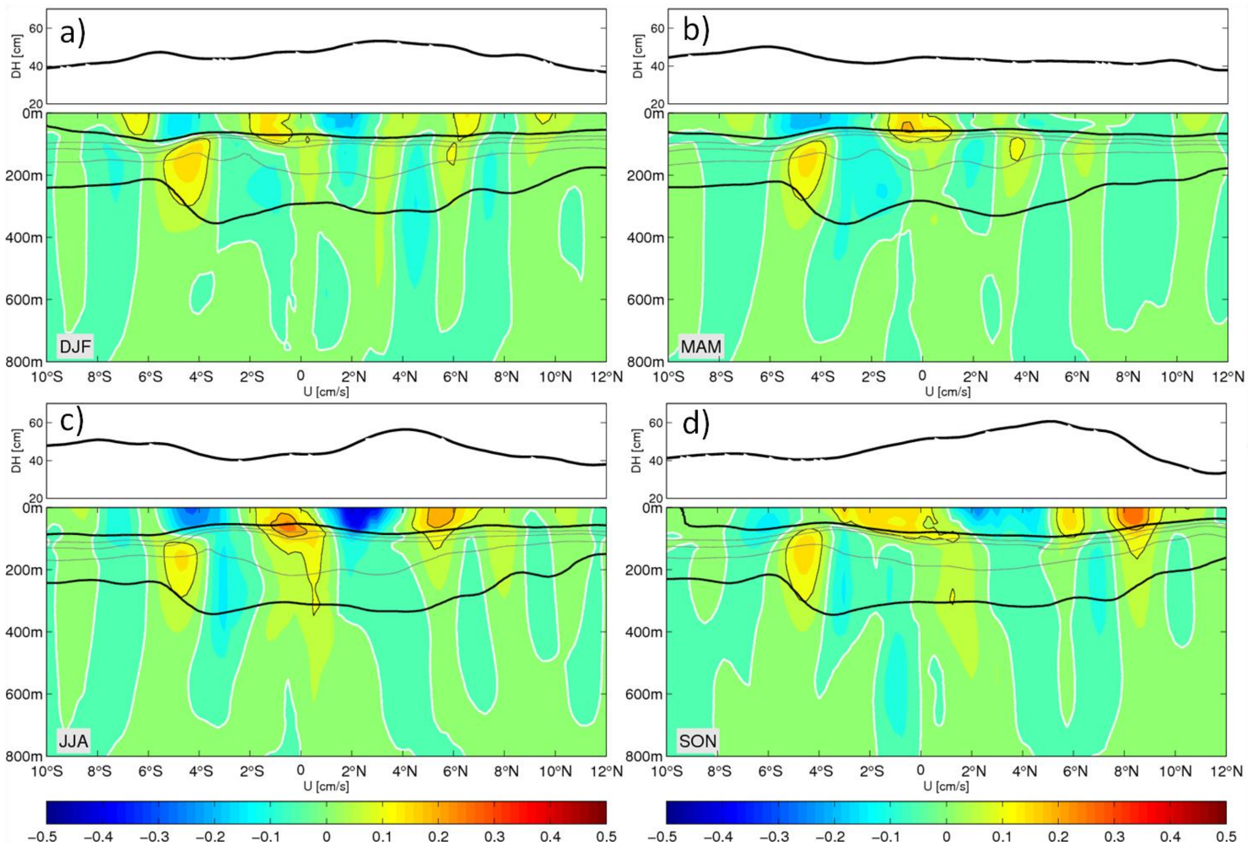

Figure 3: Mean seasonal cross-sections of velocity derived from XBT data within the months of a) Dec, Jan, Feb, b) Mar, Apr, May, c) Jun, Jul, Aug, d) Sep, Oct, Nov. The black lines along each section are the depth of the seasonal mean depths of 24.5 and 26.8 isopycnal. The top panel of each subfigure is the seasonal mean absolute dynamic height.

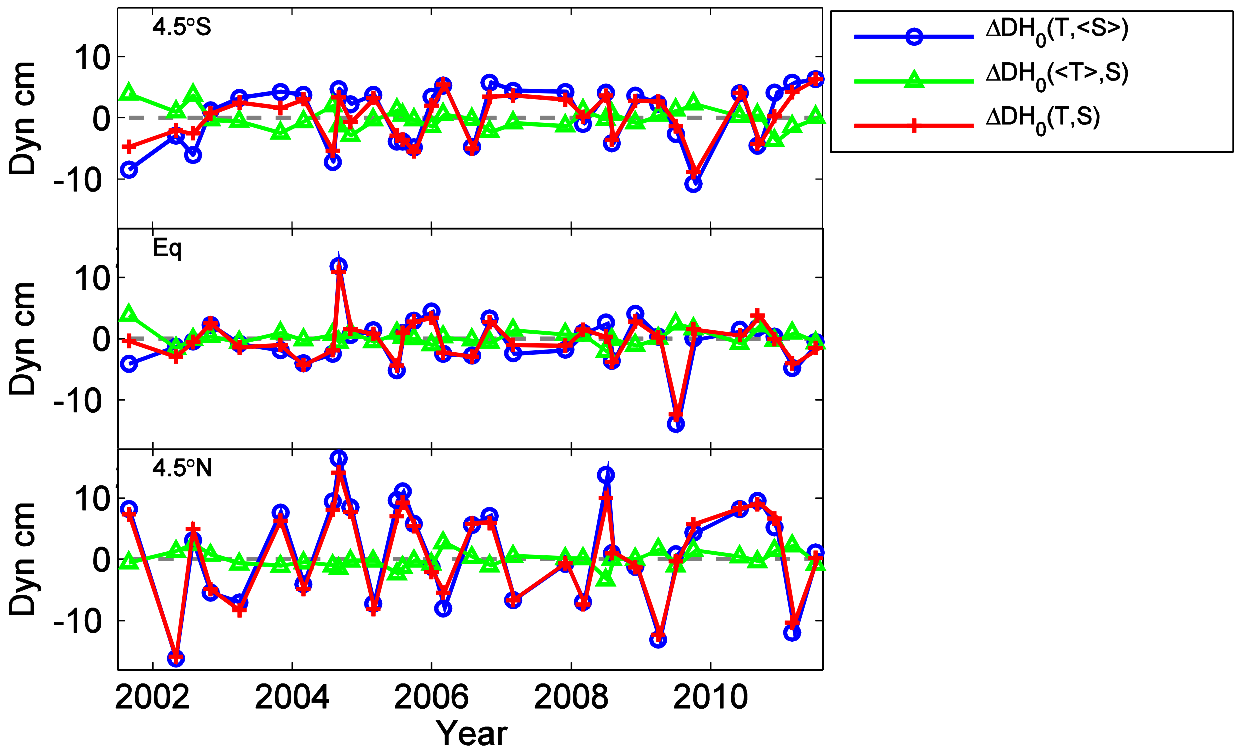

Figure 4: Anomalies of surface DH (DH_0') with respect to the annual mean of the XBT data (red) and their components thermosteric (blue) and halosteric (green). The three panels are for different latitudes, 4.5°S (upper), 0°S (middle), and 4.5°N (lower).

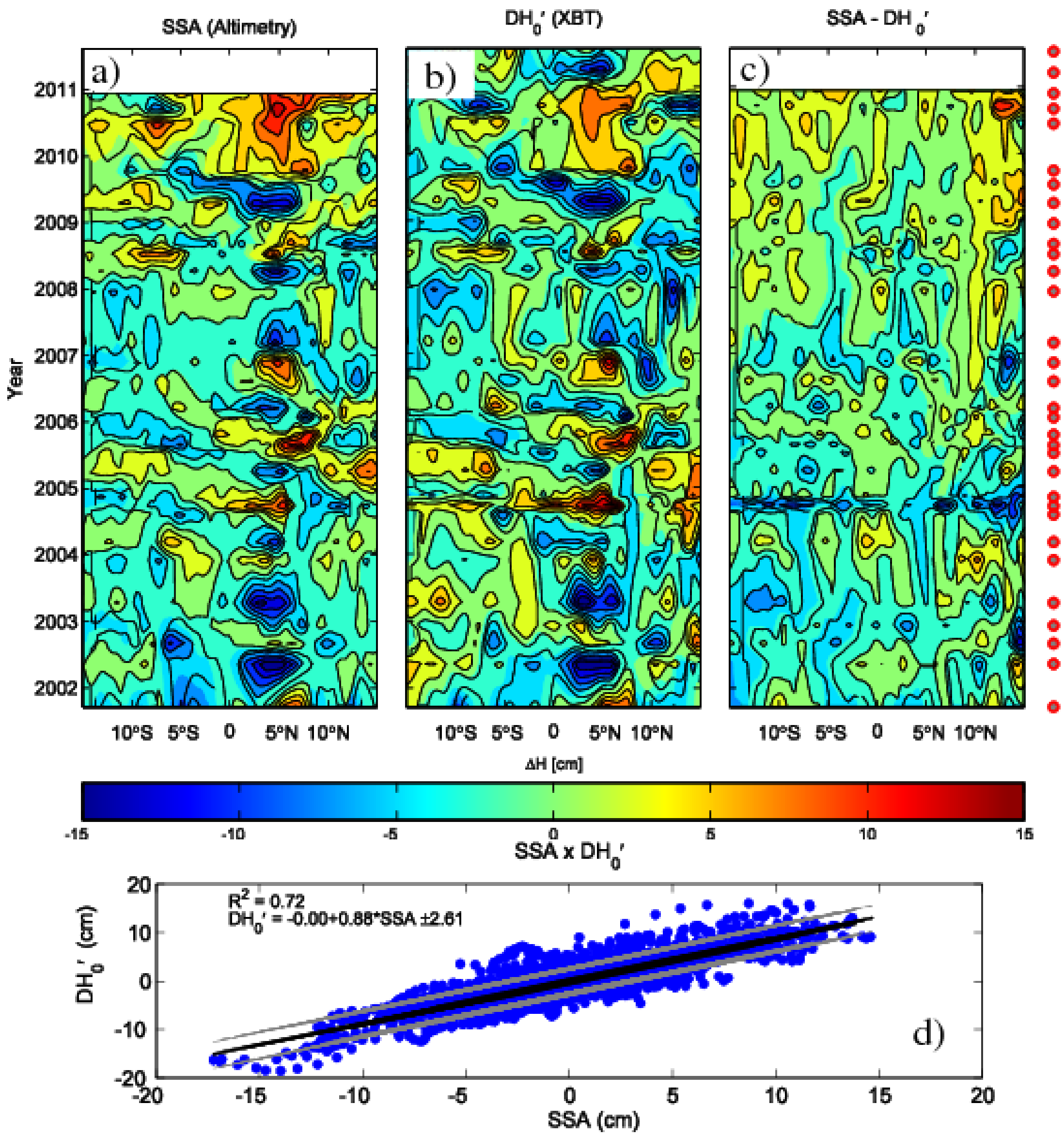

Figure 5: Comparison between SSA and surface dynamic height anomalies (DH_0’) from hydrography. Top panels: longitude-time diagrams of (a) SSA, (b) DH_0’, and (c) SSA - DH_0’. Dots on the right-hand side of the figure mark the realizations of the XBT transect. Bottom panel: (d) linear fit between DH_0’ and SSA.

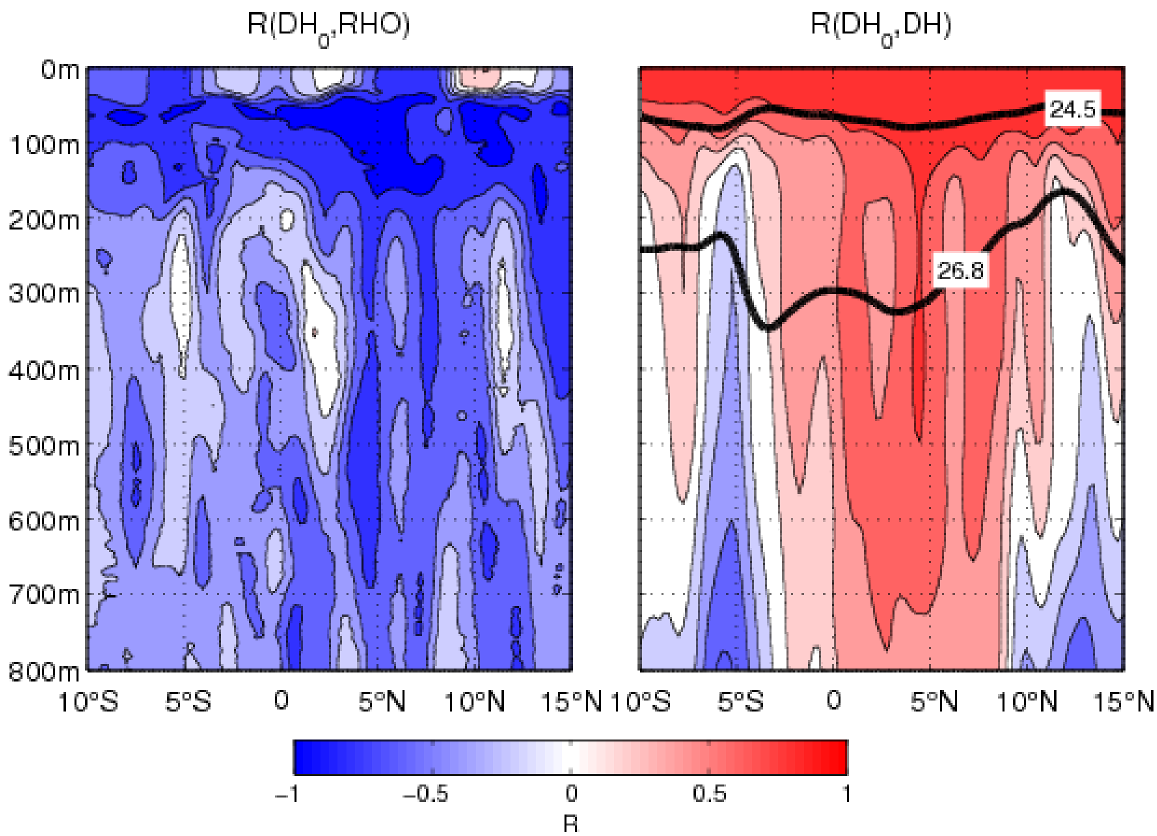

Figure 6: Correlation at each depth and latitude between the dynamic height anomalies (cm) at the surface (DH_0) and: a) density anomalies (σ_θ; kg m^{-3}) and b) dynamic height anomalies (DH'). The thick black lines in b) mark the mean location of the isopycnals σ_θ =24.5 kg m^{-3} and σ_θ = 26.8 kg m^{-3} that define the upper and lower dynamic layers used in this study.

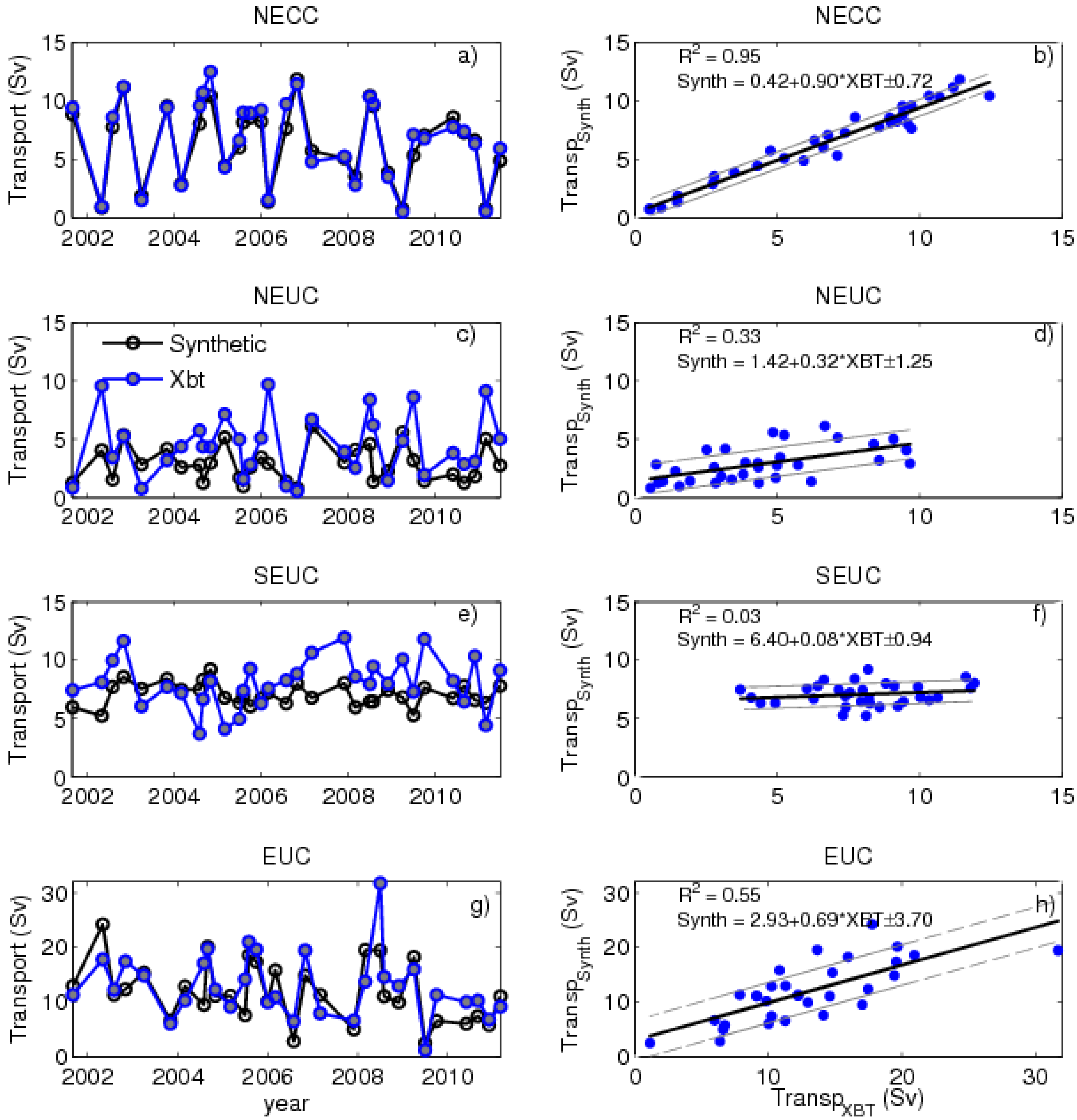

Figure 7: Left: geostrophic transports estimated by the synthetic method (black line with open dots) and transports estimated using XBT data (blue dots) for (a) NECC, (c) NEUC, (e) SEUC, and (g) EUC. Right: corresponding linear fit between the two transports estimates.

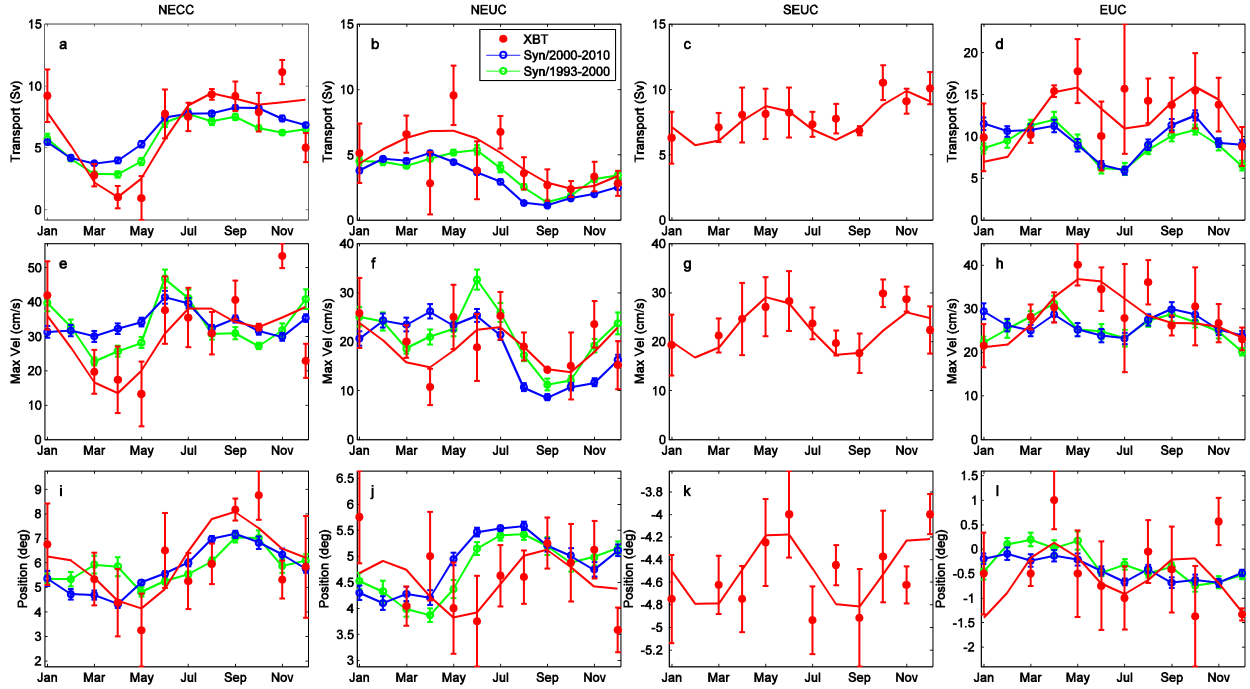

Figure 8: Climatology of geostrophic transport (Sv) (upper), maximum velocity (cm/s) (middle), and latitudinal position (deg) (lower) for the NECC (a,e,i), NEUC (b,f,j), SEUC (c,g,k) and EUC (d,h,l). Red dots are monthly XBT averages and red line represents the corresponding fit of first and second harmonics (Foltz et al., 2004a) for the XBT measurements; green/blue lines mark the average synthetic estimates for the period 1993-2000/2000-2011. The errorbars are the standard errors for the synthetic estimates, and the standard error plus fitting error as calculated in Foltz et al. (2004a).

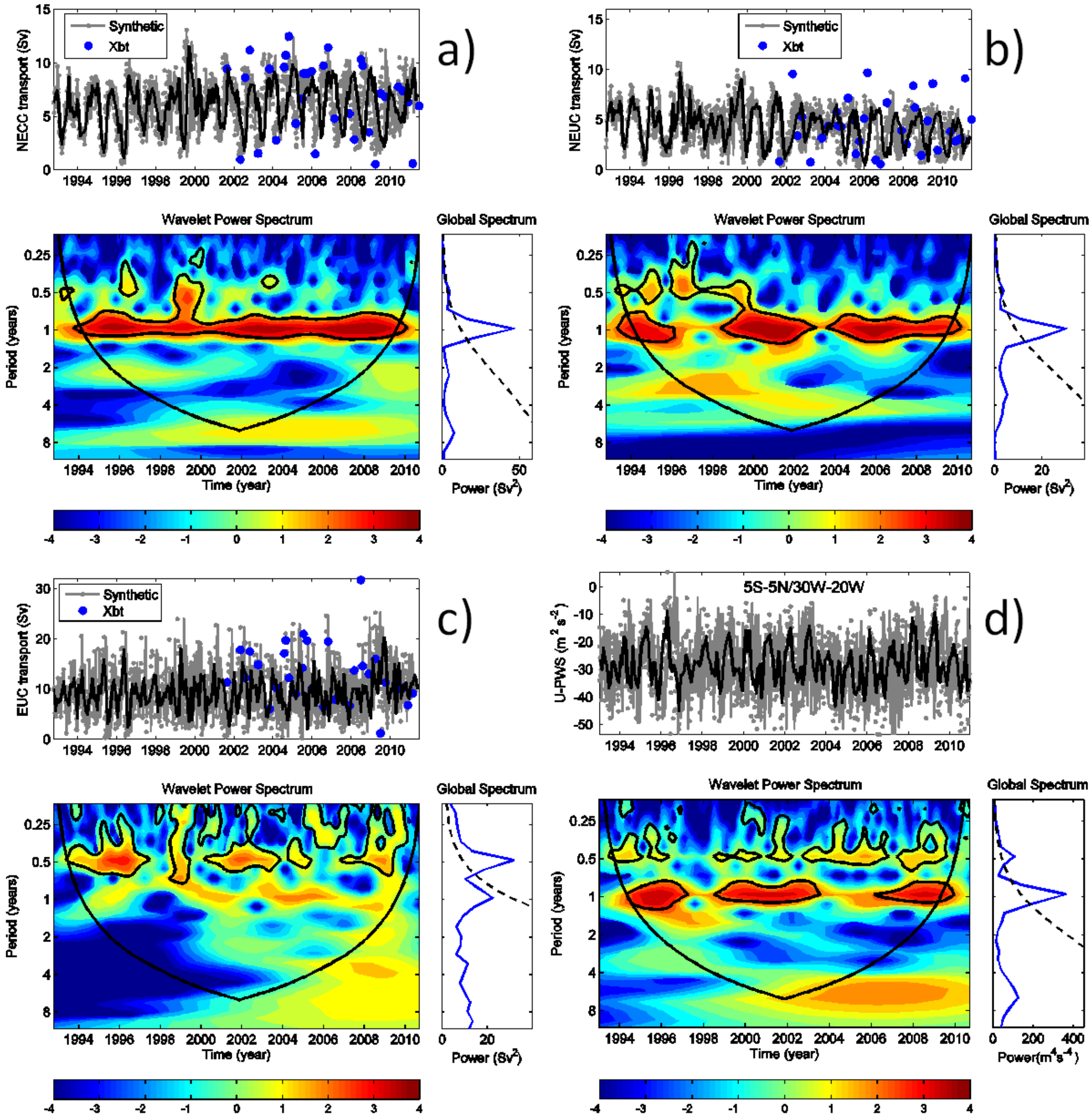

Figure 9: Time series and respective wavelet transforms for transport of (a) NECC, (b) NEUC (c) EUC, and d) zonal pseudo-wind stress averaged inside the 5S-5N/30W-20W box. The current transport timeseries (a, b, and c) are generated using the synthetic method (gray) with the discrete XBT estimates plotted on top of each timeseries (blue dots). The monthly means timeseries (black) are overlaid on each timeseries. The wavelet power spectra are based on a Morlet transform on the monthly timeseries and are shown in the contour plots underneath their respective timeseries. The wavelet power spectrum panels show the regions above the 95% significance level bounded by black closed contours, and the bowl-shaped black lines are the cone of influence above which the spectral values can be considered. Also plotted are the global averages of the wavelet spectrum (blue) and respective significance level (black dashed), as a right side panel of each wavelet power spectrum.

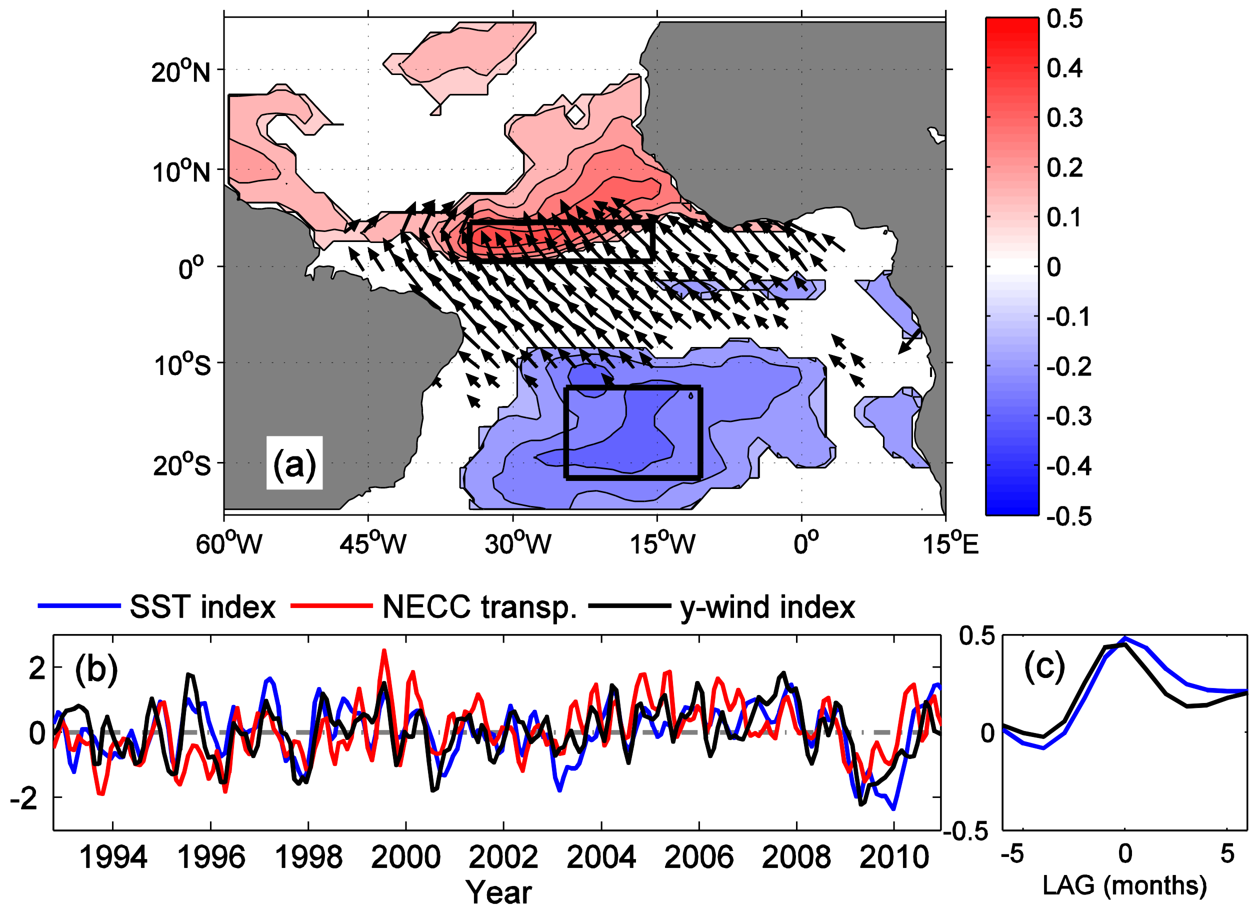

Figure 10: a) Instantaneous correlation between the NECC transport anomalies timeseries with SSTA (color) and CCMP pseudo-wind stress anomalies (arrows). Only the values that are statistically significant are shown. b) Time series of the standardized NECC transport anomalies (red), the SSTA index (blue), and the meridional wind index (y-wind; black). The SSTA index defined by subtracting the averages within the northern box (35°W-17°W/0-7°N) and the southern box (30°W-15°W/11°S-23°S) as marked in the panel a), and the y-wind index is defined as the average of the meridional pseudo-wind stress anomalies inside the northern box. c) Lagged correlation between the NECC index with the SST index (blue) and the y-wind index (black).

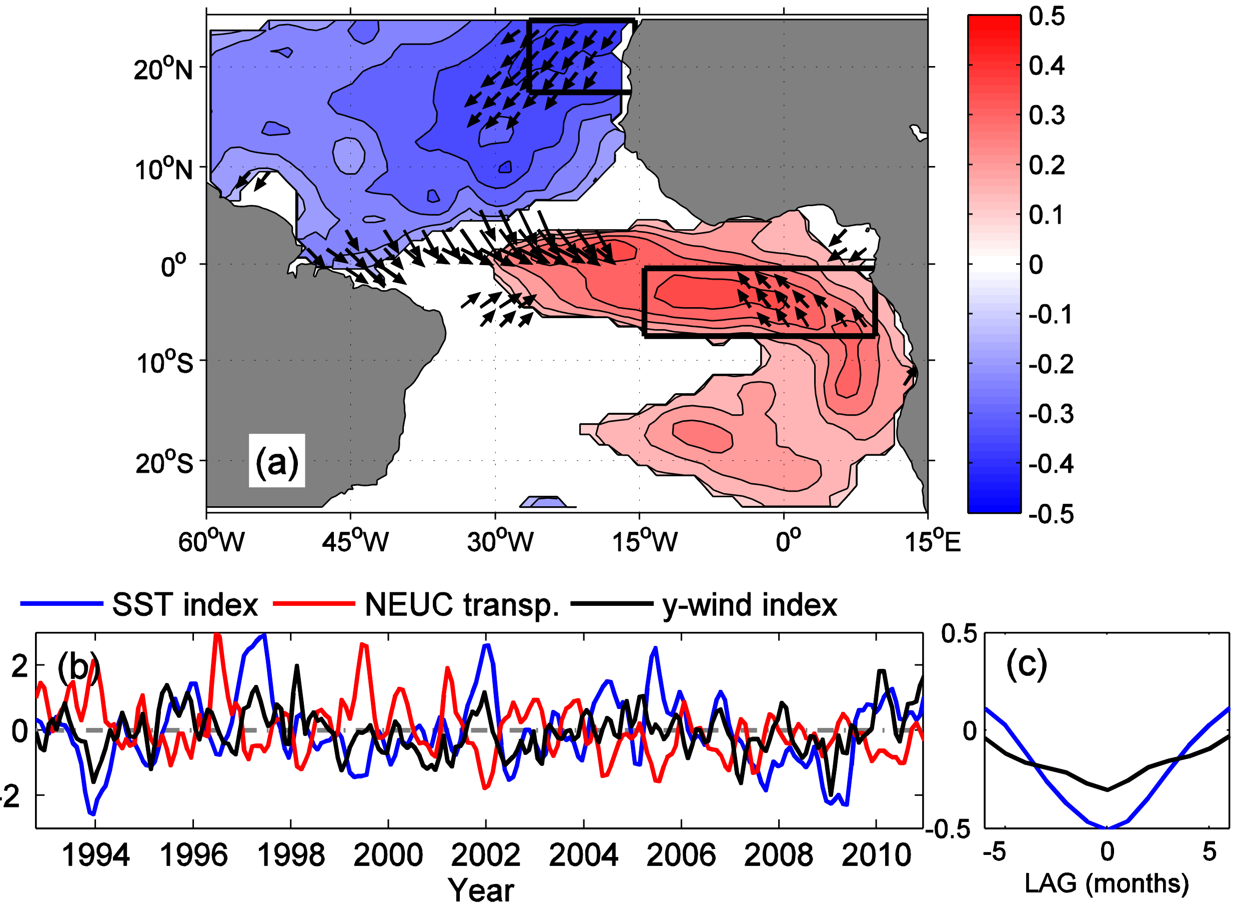

Figure 11: a) Same as figure 9a, but for NEUC transport anomalies. In b) and c) the time series of the SSTA index (blue) is defined as the difference between the northern box over the Guinea Dome region (15°-25°N/15°-30°W) and the southern box (8S-0/15W-10E), and the y-wind index is defined for the northern box as marked in panel a).

Table 1: Percentage of the variance of transport, core velocity, and position explained by the annual and semi-annual harmonics for each current using XBT estimates, and synthetic method for the 1990-2000 mean (S1990-2000) and 2000-2011 mean (S2000-2011). The synthetic method is not analyzed for the SEUC.

Current	Data	Transport (%)		Velocity (%)		Position (%)	
		Annual	Semi-ann	Annual	Semi-ann	Annual	Semi-ann
NECC	XBT	61	12	34	18	50	15
	S/1990-2000	78	17	3	70	60	20
	S/2000-2011	92	4	27	23	99	0.1
NEUC	XBT	54	1	1	49	11	26
	S/1990-2000	72	26	25	63	75	21
	S/2000-2011	99	1	87	5	78	1
SEUC	XBT	11	90	8	92	1	58
EUC	XBT	25	80	72	17	8	34
	S/1990-2000	10	81	15	75	58	18
	S/2000-2011	30	55	8	40	83	8